



UNIVERSITY OF LEEDS

This is a repository copy of *Boron-nitride/carbon-nanotube hybrid aerogels as multifunctional desulfurisation agents*.

White Rose Research Online URL for this paper:

<https://eprints.whiterose.ac.uk/151264/>

Version: Accepted Version

---

**Article:**

Xia, D, Li, H, Huang, P et al. (4 more authors) (2019) Boron-nitride/carbon-nanotube hybrid aerogels as multifunctional desulfurisation agents. *Journal of Materials Chemistry A*, 7 (41). pp. 24027-24037. ISSN 2050-7488

<https://doi.org/10.1039/c9ta06599g>

---

© The Royal Society of Chemistry 2019. This is an author produced version of a paper published in *Journal of Materials Chemistry A*. Uploaded in accordance with the publisher's self-archiving policy.

**Reuse**

Items deposited in White Rose Research Online are protected by copyright, with all rights reserved unless indicated otherwise. They may be downloaded and/or printed for private study, or other acts as permitted by national copyright laws. The publisher or other rights holders may allow further reproduction and re-use of the full text version. This is indicated by the licence information on the White Rose Research Online record for the item.

**Takedown**

If you consider content in White Rose Research Online to be in breach of UK law, please notify us by emailing [eprints@whiterose.ac.uk](mailto:eprints@whiterose.ac.uk) including the URL of the record and the reason for the withdrawal request.



[eprints@whiterose.ac.uk](mailto:eprints@whiterose.ac.uk)  
<https://eprints.whiterose.ac.uk/>

# BORON-NITRIDE/CARBON-NANOTUBE HYBRID AEROGELS AS MULTIFUNCTIONAL DESULFURISATION AGENTS

*Dong Xia,<sup>a</sup> Heng Li,<sup>b</sup> Peng Huang,<sup>c</sup> Jamie Mannering,<sup>a</sup> Alexander Kulak,<sup>a</sup> Umair Zafar,<sup>d</sup> Daniel Baker,<sup>e</sup> and Robert Menzel<sup>\*a</sup>*

## ABSTRACT

Boron nitride particles were hybridised with electrically-conducting carbon nanotube aerogels to produce electrically-heatable sorbents for commercially-important adsorptive desulfurization applications. Specifically, carbon-doped boron nitride structures (BN) were embedded within carbon nanotube (rCNT) aerogels by freeze-drying of aqueous BN-precursor/CNT mixtures followed by high-temperature thermal treatment. The resulting BN/rCNT aerogels showed considerably enhanced desulfurisation performance compared to pure BN powders, as evidenced by a 50% increase in organosulfur uptake (up to 43 mg-S/g BN) and dramatically improved sorbent regeneration stability (90% performance retention after 5 regeneration cycles). The improved desulfurisation performance was linked to substantially increased meso-porosity and improved boron-sulfur interactions in the hybrid BN/rCNT hybrid aerogels as characterised via electron microscopy, BET, EDX mapping and post-sorption XPS. Importantly, the conductivity of the CNT scaffold enabled resistive heating of BN to very high temperatures (up to 700 °C) at low energy inputs and at very high heating rates (up to 74 °C/s). The utility of resistive scaffold heating was demonstrated for energy-efficient thermal regeneration of exhausted BN/rCNT adsorbents over multiple regeneration cycles. The study demonstrates the essential advantages of hybridising BN with 3D nanocarbon networks, enhancing existing functional BN properties (sorption capacity, regeneration stability) while also introducing additional new functions (direct electrical framework heating). These findings therefore have clear implications for a wide range of BN applications, including water treatment, carbon capture, energy storage and electro-catalysis.

## INTRODUCTION

Boron nitride materials have attracted increasing attention over recent years due to a combination of unique features, including excellent mechanical properties,<sup>1</sup> high thermal conductivity and stability,<sup>2</sup> high resistance to oxidation,<sup>3</sup> and interesting catalytic properties. BN in different material forms (powders, nanotubes, nanosheets, films, membranes) are intensely investigated for a wide range of applications,<sup>4</sup> including field emitters,<sup>5</sup> optoelectronic nanodevices,<sup>6</sup> water treatment,<sup>7</sup> and catalysis.<sup>8</sup> It has been shown that combining BN with nanocarbons, such as graphene or carbon nanotubes (CNT), produces interesting heterostructures, that can be utilised, for example, as highly efficient BN/nanocarbon hybrid electrodes in supercapacitors<sup>9</sup> and Li-S batteries.<sup>10</sup> However, the study of BN/nanocarbon hybrids has been mainly restricted to powders and films, so far. The incorporation of BN into nanocarbon aerogels is investigated rarely and has so far been restricted to studies of mechanical and electro-thermal properties. Examples include the decoration of graphene oxide aerogels with exfoliated commercial BN for enhanced thermal conductivity,<sup>11</sup> the reinforcement of CNT aerogels with thin BN nanosheets to enhance mechanical aerogel strength,<sup>12</sup> and the fabrication of BN/GO hybrid aerogels for thermo-electric energy conversion applications.<sup>13</sup>

This study will focus on the synthesis of electrically-conducting BN/nanocarbon hybrid aerogels for application in adsorption desulfurisation (ADS). Desulfurisation, i.e. the removal of organosulfur compounds from hydrocarbon fuels, is a crucial pre-requisite for the operation of sulfur-sensitive fuel technologies (e.g. fuel cells) and for the reduction of environmentally harmful SO<sub>x</sub> emissions.<sup>14-16</sup> Adsorption-based desulfurization has been shown to be highly energy-efficient and particularly well-suited for the removal of aromatic and sterically-hindered organosulfur contaminants (e.g. dibenzothiophene

(DBT), dimethyldibenzothiophene (DMDBT)) that are challenging to tackle via more conventional catalytic processes (hydrodesulfurisation, oxidative desulfurisation).<sup>17</sup> A variety of materials have been shown to exhibit good adsorption desulfurisation performance, including BN,<sup>15</sup> Y-zeolite,<sup>18</sup> Cu<sub>2</sub>O,<sup>19</sup> Cu-based MOFs,<sup>20</sup> and nickel-based adsorbents.<sup>21</sup> Porous carbon materials, such as activated carbons, MOF derived carbons and N-doped porous carbons, have also shown excellent organosulfur capacities,<sup>22-24</sup> however BN powders typically exhibit more selective and faster organosulfur uptake. BN desulfurization adsorbents are typically synthesised via high-temperature reaction of boric acid with organic, nitrogen-rich precursors (e.g. melamine, dicyandiamide, urea).<sup>25</sup> Examples include urea-derived BN powders consisting of few-layers BN nanosheets (high DBT adsorption capacity, good reusability)<sup>26</sup> and melamine-derived mesoporous BN powder adsorbents with very high surface areas.<sup>25</sup> For many commercial ADS applications, the ability to regenerate exhausted desulfurisation adsorbents is crucial.<sup>27</sup> BN-based ADS studies commonly employ solvent-based regeneration strategies (adsorbent washing with hot organic solvents),<sup>26</sup> which are slow, energy-intensive and produce large amounts of organic solvent waste. Alternative thermal regeneration (adsorbent heating in air or inert atmosphere) is in principle a greener approach with greater compatibility with existing technologies.<sup>28</sup> However, traditional thermal regeneration depends on external adsorbent heating, e.g. in an oven or muffle furnace, associated with high energy consumption and large thermal gradients.<sup>29</sup>

This study will explore how hybridising BN with nanocarbon aerogels can be exploited to enhance the desulfurisation performance of BN, while also adding new functionality, such as electrical conductivity, not available in pure BN materials. It has been repeatedly shown that the functional performance of catalytic and adsorbent nanoparticles (metal, metal oxide etc.) can be improved by supporting them within nanocarbon aerogels (e.g. resulting in higher activity in heterogeneous catalysis, higher efficiency in water treatment etc.).<sup>30-32</sup> However, similar investigations on supporting functional BN particles within nanocarbon aerogels have not yet been reported. Our study will introduce a facile synthetic approach for the in-situ formation of BN within carbon nanotube aerogels, followed by detailed materials characterisation and assessment of adsorptive desulfurisation performance. (organosulfur uptake capacity, selectivity, regenerability). The electrical conductivity of the hybrid materials (not available in pure, electrically-insulating BN adsorbents) will be utilised for energy efficient BN regeneration post-adsorption, a crucial feature for the practical application of desulfurisation agents.

## **MATERIALS AND METHODS**

**Materials** Carboxylic-acid-functionalized multi-walled carbon nanotubes (oCNT), boric acid, biphenyl (BP), dibenzothiophene (DBT), dimethyldibenzothiophene (DMDBT), carbon disulfide (CS<sub>2</sub>), thiophene (TP) and 2,3-dimethylbenzothiophene (DMBT) were purchased from Sigma-Aldrich. Melamine was purchased from Alfa Aesar, UK. Ethanol, HPLC water and n-octane solvents were purchased from Scientific UK, respectively. All chemicals were used without further purification.

**BN/rCNT aerogel synthesis** The BN/rCNT hybrid aerogels were synthesised as depicted in Figure 1. Typically, commercial oxidised CNT (oCNT, 0.075 g) were dispersed in 10 mL water/ethanol solution via ultrasonic probe sonication (4 × 5 min, 30% of ultrasound power, model HD 2200, Bandelin sonopuls). Then boric acid (0.1315 g, 0.0021 mole) was added to the oCNT dispersion and sonicated, followed by the addition of melamine (0.5365 g, 0.0042 mole). The resulting mixture was probe sonicated for 4 × 5 min. The resulting boric-acid/melamine/oCNT mixture was frozen and freeze-dried for 24 h within bespoke cylindrical moulds. Freeze-drying yielded a freestanding, cylindrical boric-acid/melamine/oCNT aerogel monolith that was thermally treated in a tube furnace (Carbolite Gero Limited) at 1000 °C for 2 h under a nitrogen atmosphere at a heating rate of 5 °C/min to convert the small molecule precursors into BN. The resulting hybrid aerogel (BN/rCNT aerogel) had a nominal BN weight loading of 40 wt%. Other aerogels with BN loadings of 2.5 wt% and 10 wt%, were prepared by adjusting the boric acid and melamine concentrations in the procedure

above. To produce a pure BN reference sample ('BN powder'), the BN precursors, boric acid (0.619 g, 0.01 mole) and melamine (2.53 g, 0.02 mole), were dissolved in 40 mL water/ethanol solution (volume ratio 1:1) and heated at 50 °C to dryness. The resulting solid boric-acid/melamine mixture was ground into a fine powder and then thermally treated under conditions described above.

Adsorption measurements The adsorbents were tested via batch adsorption experiments. All model fuels were prepared by dissolving a desired amount of organosulfur in pure n-octane. Unless otherwise stated, standard experiments were carried out at room temperature, using dibenzothiophene (DBT) as model organosulfur compound at a concentration of 500 ppm sulfur. For a standard adsorption experiment, the adsorbent (0.05 g) was added to the DBT solution and agitated at room temperature for 3 h, using a magnetic stirrer bar or an orbital shaker (Stuart SSL1, UK, 120 rpm/min). Each adsorption measurement was accompanied by a pure reference solution to account for potential non-adsorbent-related variations in DBT concentration. All sampled DBT solutions were centrifuged to sediment potential particle impurities. The DBT concentration was then measured via gas chromatography (GC) using a Agilent 7890B GC system with a HP-5 column (0.32 m diameter, film thickness of 0.25 µm, 30 m in length, working temperature from 25 to 300 °C). The amount of adsorbed DBT was calculated from the reduction in organosulfur GC peak area relative to the pure DBT reference. The effect of temperature on DBT sorption was tested at 25 °C, 50 °C, and 80 °C respectively. To determine adsorption kinetics, samples were agitated for 3 h and solution aliquots (0.6 mL) were sampled at defined time intervals. For the adsorption isotherms, DBT sorption was tested, using a range of initial DBT concentrations (100, 200, 300, and 500 ppm S). Organosulfur selectivity testing was carried out using mixtures of DBT and biphenyl (BP) in n-octane (500 ppm sulfur DBT, 2873 ppm BP). The simultaneous adsorption of DBT and 4,6-dimethyldibenzothiophene (DMDBT) was measured at a total sulphur concentration of 500 ppm sulfur (i.e. using a mixture of 250 ppm sulfur DBT and 250 ppm sulfur DMDBT). Additional experiments were carried out to explore the uptake of other organosulfur compounds, including carbon disulfide (CS<sub>2</sub>), thiophene (TP) and 2,3-dimethylbenzthiophene (DMBT). These experiments were carried using the respective pure organosulfur compound in n-octane solution at an initial concentration of 500 ppm S.

Joule-heating of aerogel adsorbents A customized set-up, enabling to connect monolithic aerogels to an electrical current via aluminium electrodes and measure their core temperature via a thermocouple, was used for direct resistive heating (Joule heating) of the BN/rCNT aerogels (Figure 2). To protect the samples during high-temperature Joule-heating (i.e. during heating above 320°C), the set-up was placed in a custom-made airtight container that allowed connection to an external power source and constant flow of inert nitrogen gas (100 mL/min) during the heating experiments. Using this setup, BN/rCNT aerogels were electrically heated between 50-750 °C. To measure accurate Joule-heating characteristics, the electrical current through the aerogel was adjusted until a set temperature was reached. The sample was then left to equilibrate, before recording voltage and current. This procedure was repeated to heat the aerogel in 50 °C steps. Prior to a measurement series, the aerogel samples were preconditioned (Joule-heating to 200 °C for 20 min) in order to desorb any undesired impurities (e.g. water, CO<sub>2</sub> etc, see ESI Fig. S15) and obtain stable Joule-heating readings. For thermal aerogel regeneration post-adsorption, the BN/rCNT aerogels were removed from the organosulfur solution and mildly dried at 50 °C to remove residual n-octane. The BN/rCNT aerogels were then electrically heated to 400 °C for 1 h. After Joule heating regeneration, the intact aerogel was immersed into fresh DBT solution and the Joule heating procedure was repeated for five regeneration cycles.

Material characterisation Powder X-ray diffraction (XRD) were performed on a Bruker D2 Phaser Diffractometer using CuK $\alpha$  radiation. Infrared spectroscopy (IR) was carried using a PerkinElmer Spectrum One IR Spectrometer, with the scanning range between 550 and 4000 cm<sup>-1</sup>. Thermogravimetric analysis (TGA Q600 model, USA) was carried out in air atmosphere between 20-850°C at a ramping rate of 10

oC/min. Nitrogen sorption isotherms were collected using a Micrometrics TriStar 3000 and analysed using TriStar 3000 (V6.04) software. Scanning electron microscopy (SEM) images were taken on a Nova NanoSEM 450 with an accelerating voltage of 3 kV. Energy dispersive X-ray (EDX) mapping was performed on the same equipment, using an accelerating voltage of 18 kV. SEM samples were fixed onto alumina stubs using conducting copper tape and coated with a 2 nm Ir conductive layer before analysis. Transmission electron microscopy (TEM) images were performed on an electron microscope (Tecnai F30, FEI) at an accelerating voltage of 300 kV. Samples were sonicated in ethanol, followed by drop-casting onto a copper grid. Raman spectroscopy was conducted using a Renishaw InVia with an excitation laser wavelength of 532 nm between 400 and 4000  $\text{cm}^{-1}$ . X-ray photoelectron spectroscopy (XPS) analysis was performed on a K-Alpha+ X-ray photoelectron spectrometer (Thermo Fisher Scientific), using focused (400  $\mu\text{m}$  spot) monochromatic Al-K $\alpha$  radiation. The binding energies were referenced to the C1s peak of adventitious carbon at 284.8 eV. The mechanical compressibility was tested using an Instron 5566 serials mechanical testing machine at a loading speed 1 mm/min. The electrical conductivity was measured within the Joule-heating setup. The thermal conductivity of aerogel sample was estimated from the thermal Joule-heating gradient of an uninsulated aerogel sample, using a previously reported methodology.<sup>33</sup>

## RESULTS AND DISCUSSION

### BN/rCNT aerogel synthesis and characterisation

BN/rCNT hybrid aerogels were produced from a dispersion of commercially-available, acid-oxidised multi-walled carbon nanotubes (oCNT) in a solution of simple molecular BN precursors (boric acid and melamine in a nominal molar ratio 1:2), as shown in Figure 1. As solvent a 1:1 water/ethanol mixture was used to ensure solubility of the molecular precursors while maintaining a high solvent polarity, crucial for the exfoliation of the oCNT. At the relatively high precursor and oCNT concentrations used, thorough dispersion results in the formation of an oCNT network infused with the BN precursors. The resulting wet-gel withstands lyophilisation to form a stable oCNT/boric-acid/melamine aerogel. Subsequent high-temperature treatment in inert atmosphere is used to convert the molecular precursors into BN and to thermally reduce the oCNT into electrically-conducting reduced CNT (rCNT), forming monolithic BN/rCNT aerogels (Fig. 3a). Initial optimisation studies focused on the variation of the BN:CNT ratio to improve the structural integrity of the final hybrid aerogels, a crucial prerequisite for the practical application of the aerogel materials. Hybrid aerogels with different nominal BN weight percentage were produced. While BN weight ratios of 2.5 wt% and 10 wt% yielded free-standing aerogel monoliths, their structure was relatively fragile (ESI, Fig. S1). However, aerogels consisting of 40 wt% BN and 60 wt% rCNT showed excellent mechanical robustness (able to support about 4000 times their own weight, see Fig. 3a) and were taken forward for subsequent materials characterisation and desulfurisation testing. It is worth noting that BN weight ratios larger than 40 wt% could not be accessed in our synthetic approach due to solubility limitations of the molecular BN precursors. It is further worth noting that precursor conversion at lower temperatures yielded BN/rCNT sorbents with reduced performance (see ESI, Fig S8).

The hybrid aerogels with a nominal BN weight ratio of 40 wt% (for the remainder of the paper referred to as BN/rCNT aerogels for simplicity) were characterised and tested in more detail. The actual BN weight ratio in the hybrid aerogel was estimated by TGA to be 39 wt% (see ESI, Fig. S2), very close to the intended nominal weight ratio, indicating full precursor conversion and efficient removal of any by-products during the thermal conversion treatment. Raman spectroscopy confirmed graphitisation of the CNT network after the thermal treatment, as indicated by a significant increase of the IG/ID ratio from 0.68 to 0.87 (ESI, Fig. S3).

In order to confirm the formation of BN during thermal treatment, the BN/rCNT aerogels as well as a pure BN powder control sample were characterised by XRD, IR and XPS spectroscopy. The XRD pattern of the BN

powder showed two broad diffraction peaks at 26° and 43° (Fig. 3b), corresponding to the (002) and (100) lattice planes of BN and consistent with the formation of turbostratic and/or amorphous BN.<sup>34,35</sup> For the BN/rCNT aerogel, the strong graphitic (002) diffraction of the rCNT,<sup>36</sup> potentially obscures the BN peak at 26°. Therefore, IR spectroscopy was used to further confirm BN formation (Fig. 3c). Both BN powder as well as BN/rCNT aerogel exhibit two characteristic IR bands at around 1370 cm<sup>-1</sup> and 801 cm<sup>-1</sup>, corresponding to the in-plane B–N stretching vibrations and out-of-plane B–N–B bending vibrations, respectively,<sup>37</sup> providing clear evidence for the formation of BN in both samples.

X-ray photoelectron spectroscopy (XPS) was carried out to quantify elemental composition and chemical binding state (Fig. 3f). XPS survey spectra confirmed the presence of B and N, further confirming successful precursor conversion into BN. XPS also indicates the presence of carbon and oxygen defects in the BN powder sample (ESI, Fig. S4), consistent with reported studies.<sup>15,35,37</sup> This observation suggests that our synthetic approach generates carbon-doped BN (with some of the carbon associated with residual oxygen), which has been repeatedly observed in the literature when forming BN from melamine precursors under conditions comparable to ours.<sup>15,38</sup> In fact, carbon-doped BN samples have been shown to be outstanding adsorbents, rendering the synthesised hybrid aerogels highly promising for adsorptive desulfurisation applications.<sup>15</sup> High-resolution XPS scans in the B1s region and N1s regions give further insight into changes in chemical binding state of BN. For the un-hybridised BN powder (Fig. 3f), the high-resolution B1s spectrum exhibits two characteristic peaks, related to B–N (190.68 eV) and B–O–N (191.67 eV), consistent with literature findings on doped BN.<sup>38,39</sup> In the BN/rCNT aerogel, these B–N (191.31 eV) and B–O–N (192.66 eV) binding energies shift to higher energies indicating charge transfer between rCNT and BN.<sup>35,40</sup> Further a new peak emerges, which is assigned to B–C binding, suggesting a degree of covalent binding between BN and rCNT. The high-resolution N1s spectra show a very similar behaviour (Fig. 3f). For the BN powder only the characteristic B–N peak (398.20 eV) is observed.<sup>39</sup> For the BN/rCNT aerogel however, an additional shoulder (398.92 eV) emerges, attributable to C–N binding.<sup>37</sup> These XPS findings provide clear evidence that BN and rCNTs are in intimate contact within the hybrid aerogels and that some degree of covalent cross-linking between the BN and rCNT structures has occurred during the high-temperature synthesis.

Scanning electron microscopy (SEM) and energy dispersive X-ray (EDX) mapping were performed to visualise the internal structure and elemental distribution of the synthesized materials (Fig. 4). The BN powder consists of micrometer-sized whisker-like particles (Fig. 4a), in line with melamine-derived BN adsorbents previously described in the literature.<sup>34,35</sup> The BN particles in the CNT-free BN powder are heavily aggregated, due to sintering during the high-temperature conversion process. EDX mapping confirms that the BN structures are carbon-doped, showing a uniform distribution of boron, nitrogen and carbon throughout the BN rod structures (Fig. 4a1-a4). TEM of the corrugated edges of some thinner BN structures (ESI, Fig S6) indicate the presence of very small pores (< 5 nm) within the BN structures. For BN/rCNT aerogels, SEM imaging shows BN particles of similar elongated morphology as in the BN powder but with smaller diameter and considerably less aggregated (Fig. 4b). SEM also shows that the BN structures are in intimate contact with the rCNT (Fig. 4b) and well embedded within the CNT network (Fig. 4b1-b3). TEM images of the BN/rCNT aerogel fragments (ESI, Fig. S7) further confirm that that the BN structures are fully embedded within a porous, mesh-like network of multi-walled CNT.

Bulk characterisation of the materials via BET measurements (Fig. 3d and 3e) is fully consistent with the sorbent microstructures observed by electron microscopy. For the pure BN powders, the shape of nitrogen isotherm (Fig. 3d) exhibits combined characteristics of Type I and Type IV isotherms, indicating the presence of hierarchical porosity, i.e. indicating the presence of both micro-pores and meso-pores. Mesoporosity likely arises from the interstitial spaces between BN structures, while the micro-porosity observed is consistent with the very small, internal BN pores, observed by TEM (ESI, Fig S6b). The high specific

surface area of the pure BN (1000 m<sup>2</sup>/g, Table 1) further confirms the presence of significant amount of micro-porosity within the BN structures. These results are in line with literature observations on melamine-derived BN structures.<sup>34</sup> For the BN/rCNT aerogels, the shape of the nitrogen isotherm is closer to a pure Type IV form. This shape indicates a significant increase in mesopore volume compared to the pure BN powder, likely to be associated with the mesh-like morphology of the CNT network and the less aggregated morphology of the BN structures in the aerogels, as observed by SEM (Fig. 4b). In fact, BJH analysis (Fig. 3e) shows that the BN/rCNT aerogel sorbents have very large meso-pore volume ( $V_{\text{meso}} = 0.62 \text{ cm}^3/\text{g}$ ) and a relatively large, average meso-pore size ( $d_{\text{meso}} = 40 \text{ nm}$ ) – more than one order of magnitude increased, compared to the pure, unhybridised BN sorbents (Table 1). The specific surface area of the BN/rCNT aerogels is however slightly lower compared to the pure BN powder (Table 1), which might be related to a somewhat reduced micro-porosity. However, the dramatic improvements in meso-porosity substantially outweigh this slight surface area decrease, resulting in significantly improved organosulfur uptake in the highly mesoporous BN/rCNT aerogel sorbents, compared to the more aggregated, pure BN materials (Table 1).

The hybridisation of BN with CNT aerogels also impacts on other important materials properties. The interpenetration of the nanoscale rCNT network with larger, robust BN structures imparts the BN/rCNT aerogels with considerably enhanced electrical, thermal and mechanical properties, highly beneficial for sorption (and other) applications. Importantly, our hybrid BN/rCNT aerogels are electrically conducting ( $\sigma = 5.3 \text{ S/m}$  at rt, Table 1), in contrast to conventional BN sorbents that are electrically insulating. The ability to conduct electricity confirms that the rCNT network remains interconnected throughout the whole aerogel volume in the presence of the BN structures. The I-V characteristics of the BN/rCNT aerogel (Fig. 5a) show non-linear behaviour with a clear drop in electrical resistance at higher currents related to resistive heating (ESI, Fig. S14) and typical for hybridisation of electrical insulators (BN) with conductors (rCNT).<sup>41</sup> Further, the BN/rCNT aerogels exhibit excellent thermal conductivity ( $\kappa = 0.59 \text{ W}\cdot\text{m}^{-1}\cdot\text{K}^{-1}$ ), considerably higher than conventional porous sorbent materials (Fig. 5b). High thermal conductivity results in fast heat dissipation which can be highly beneficial for sorption and catalytic applications, enabling efficient dissipation of excess exothermic energy as well as rapid temperature cycling, e.g. during thermal material regeneration. The BN/rCNT aerogels also show good mechanical properties (Fig. 5c). Mechanical compressibility tests show that the BN/rCNT aerogel have a 7 times larger compressive strength (53 kPa) compared to an analogous aerogel made from only rCNT (7.5 kPa). This increase indicates that the BN structure act as mechanical reinforcements in the rCNT network, likely aided by a degree of covalent crosslinking between BN and CNT as indicated by XPS. The improved mechanical strength is a crucial prerequisite for applications, providing durable aerogel monoliths that are able to maintain structural integrity during operation and subsequent regeneration.

### **Adsorptive desulfurization**

Dibenzothiophene (DBT) adsorption from n-octane solution onto the BN/rCNT aerogels and pure BN powders was investigated to assess the adsorptive desulfurisation performance (Fig. 6a and 6b). Temperature-dependent sorption studies showed a significant drop in DBT uptake at elevated temperatures (ESI, Fig S8), indicating that DBT sorption onto BN is exothermic, as previously reported.<sup>26</sup> Consequently, all desulfurisation tests were carried out at room temperature. Organosulfur uptake kinetics onto pure and hybridised BN are relatively fast, reaching equilibrium in less than 30 min (Fig. 6a). The DBT adsorption isotherms show that, for all initial DBT concentrations tested, organosulfur uptake onto the BN/rCNT aerogels is greater than onto pure BN (Fig. 6b). For example an initial DBT concentration of 500 ppm S, the BN/rCNT aerogels show a 50% increase in DBT uptake (32 mg·S/gBN) compared to the BN powder (21 mg·S/gBN). Importantly, control experiments using pure (i.e. BN-free) rCNT aerogels confirmed that the rCNT framework itself does not significantly contribute to this increase (see ESI Fig. S10), indicating

that the capacity improvement is purely due to changes in BN morphology, including improved dispersion of BN structures and substantially increased meso-porosity in the BN/rCNT aerogels.

Both isotherms fitted very well a conventional Langmuir model ( $R^2 > 0.97$ , see ESI Table S2), suggesting the presence of a relatively homogeneous surface and the formation of a saturated monolayer. The maximum DBT uptake capacity ( $q_m$ , Table 1) of the BN/rCNT aerogels is again about 50 % higher compared pure BN, further confirming the substantial improvement in organosulfur uptake in the hybrid materials. The second Langmuir fitting parameter,  $K_L$  (related to the sorption energy) is also slightly larger (around 15 %) for the BN/rCNT aerogel (ESI table S2), which might indicate a slight increase in DBT-BN binding strength in the aerogels, potentially related to the charge transfer effects discussed earlier in the manuscript.

The DBT removal capacity of our BN/rCNT aerogels reach commercially relevant levels (in line with previous BN desulfurisation studies),<sup>25,26,35</sup> showing similar or higher performance compared to many other desulfurisation sorbents (Table 2),<sup>14, 22-24, 42, 43</sup> such as Cu<sub>2</sub>O powder,<sup>19</sup> Ni nanoparticles decorated activated carbon beads (Ni-ACB)<sup>44</sup> and commercial metal-organic frameworks (Cu-BTC).<sup>20</sup> It is worth noting that the desulfurisation sorbents listed in Table 2 (including the high-capacity N-doped porous carbon) are powders, while our BN/rCNT hybrids are monolithic aerogels. The monolithic form of our sorbent allows for much easier recovery from liquid solution, while the integrated interconnected CNT network enables direct electrical heating (not possible in loose powders), which will be studied in detail in the final section of this study.

Our BN/rCNT aerogel sorbents show also excellent desulfurization performance for other typical organosulfur impurities, including carbon disulphide, thiophene, 3,5-dimethylbenzothiophene and 4,6-dimethyldibenzothiophene, with uptake capacities (from n-octane solution) between 18 - 49 mg-S/g BN, depending on the sulfur compound (ESI, Fig. S13). In addition, our sorbents have pronounced selectivity towards organosulfurs. To provide first evidence for this, the uptake of DBT from n-octane solution was tested in the presence of dissolved biphenyl (BP),<sup>14</sup> a sulfur-free aromatic compound, structurally similar to DBT (Fig. 6d). Competitive sorption experiments using a mixture of DBT and BP in n-octane (Fig. 6d) showed only very small BP uptake while DBT uptake remains undiminishedly high (31 mg-S/gBN, Fig. 6d). However, when competitive sorption measurements were conducted using a mixture of two organosulfur compounds (mixture of DBT and DMBT in n-octane, Fig. 6c) both organosulfur compounds were adsorbed strongly, reaching a high total (combined) organosulfur uptake of 43 mg-S/g BN in the BN/rCNT aerogels (Fig. 6c). The combination of excellent selectivity towards organosulfurs and high uptake across a broad variety of sulfur compounds renders our BN/rCNT aerogels highly promising for real-life adsorptive desulfurization applications across a range of fuel types.

To rationalise the affinity of our BN materials towards organosulfurs, post-sorption analysis of the aerogel and powder adsorbents via IR and XPS was carried out to gain further insight into the underpinning sorption process. To this end, sorbents were left to equilibrate in DBT solution, then washed with n-octane at room temperature and dried. The IR spectra of the post-sorption samples showed a new characteristic band, clearly indicating the presence of firmly bound DBT molecules (ESI, Fig. S11). XPS of post-sorption BN and BN/rCNT aerogel further confirmed the presence of sulfur (Fig. 6e). Comparison between the high-resolution S<sub>2p</sub> spectrum of the post-sorption sorbents and pristine DBT powder indicates strong interactions between DBT and BN. Both post-sorption adsorbents showed an additional large shoulder in the high-resolution S<sub>2p</sub> peak that we attribute to S···B=N- binding.<sup>45</sup> A small shift is also observed in the B<sub>1s</sub> peaks post-sorption (Fig. 6f). However, no significant peak shifts are observed for the N<sub>1s</sub> XPS peaks or the C<sub>1s</sub> peaks of the carbon dopant (see ESI, Fig. S12). This observation indicates charge transfer from the lone pairs of the DBT sulfur atoms (Lewis base) to empty acceptor orbitals located at the boron atoms of BN adsorbent (Lewis acid).<sup>26,35</sup> The underpinning sorption process is therefore based on strong Lewis acid-base interactions between organosulfur and BN sorbent, with the electron-rich sulfur-containing impurities

binding through their lone pairs to the electron-deficient boron atoms in the BN structure. These findings are consistent with recent theoretical studies, investigating the binding of DBT to BN via DFT simulations.<sup>26</sup> Organosulfur sorption based on Lewis interactions is also consistent with the very low DBT uptake observed for the rCNT network, evidencing poor interactions between the electron-rich graphitic surfaces and the electron lone pairs at the DBT sulfur. The higher affinity of BN towards DMDBT compared to DBT (Fig. 6c) further confirms a Lewis acid base sorption mechanism (leading to stronger interactions between BN and DMDBT due to the increased Lewis basicity of alkyl-substituted benzothiophenes).<sup>26,46</sup>

### **Joule-heating of BN/rCNT aerogel for sorbent regeneration**

The electrical conductivity of the BN/rCNT aerogel enables direct electrical heating (Joule-heating) of the rCNT network and thereby fast and energy-efficient heating of the embedded BN desulfurisation sorbents (Fig. 7a). The BN/rCNT aerogels can be readily heated to up to 700° (in inert atmosphere) without any damage or degradation to the aerogel. The Joule-heating temperature of the BN/rCNT aerogel is linearly dependent on the electrical power input (25 °C/W, Fig. 7a), enabling to set any desired temperature by simply adjusting electrical voltage or current. Importantly, Joule-heating occurs very rapidly, exhibiting heating rates of up to 74 K/s and reaching 700°C in less than 10 s. Once the Joule-heating current is switched off, the BN/rCNT aerogels also exhibit very fast cooling rates (up to 73 K/s), enabled by their excellent thermal conductivity and associated heat dissipation properties. The hybrid aerogels show similar Joule-heating characteristics in air atmosphere where they can be heated to up to 320 °C without damage to the carbon network (see ESI, Fig. S16).

Regenerability and reusability of exhausted desulfurisation adsorbents are crucial factors for the viability of commercial desulfurisation adsorbents. As mentioned above, the monolithic form of the BN/rCNT aerogels allows very easy recovery of the adsorbent of exhausted sorbents from hydrocarbon solution, without the need for any additional separation processes (centrifugation, filtration, sedimentation), that need to be employed for powder adsorbents. The post-sorption hybrid aerogels remain electrically-conducting and can be easily regenerated via Joule heating (Fig. 8a). To this end, exhausted BN/rCNT aerogels were Joule-heated to 400 oC (Fig. 8b and ESI Fig. S17) to induce thermal DBT desorption (DBT boiling point 333 oC). The regenerated hybrid aerogels were re-used in batch DBT adsorption measurements and repeatedly regenerated. The regeneration efficiency remains close to 90 % of the initial uptake capacity over five regeneration cycles (Fig. 8c). The slight decrease in regeneration capacity after the fourth cycle is attributed to a marginal loss of sorbent material during repeated use and manual handling of the aerogel sorbents. The average energy consumption for each thermal regeneration cycle was only 0.018 kW·h (see ESI, Table S3), which is considerably lower than traditional thermal regeneration of the same sorbent through external heating in an oven or furnace. The rapid heating and cooling rates minimise the duration of the thermal regeneration step, further contributing to minimise energy consumption. For 1 kg sorbent, the energy consumption for fast, high-temperature regeneration (Joule-heating 700°C, 1 min as depicted in Fig. 7b) is estimated to be around 9 kWh/kg sorbent. The use of BN/rCNT aerogel adsorbents therefore enables highly efficient and repeatable thermal sorbent recycling at minimal energy costs via direct resistive framework heating.

### **CONCLUSIONS**

In summary, our study reports the fabrication of electrically-heatable, highly-porous BN/rCNT aerogel materials, produced via facile thermal conversion of molecular precursors within a 3D CNT network. The BN/rCNT aerogels exhibit outstanding desulfurisation properties, including large, commercially-relevant organosulfur uptake capacities, excellent organosulfur selectivity, fast uptake kinetics and high recycling

stability. Detailed materials characterisation of the BN/rCNT aerogels showed reduced BN particle sintering and increased mesoporosity compared to pure BN powder adsorbents, underpinning the improved organosulfur uptake in the hybrid aerogels. XPS measurements provided clear evidence for strong Lewis acid-base interactions between the BN adsorbent and the organosulfur adsorbates, likely giving rise to the excellent organosulfur selectivity of BN, confirming recent theoretical predictions. Joule-heating of the BN/rCNT aerogels (not possible in pure BN powders or pure BN aerogels) enabled temperature control to high temperatures (up to 700 °C) at very high heating rates (up to 74 °C/s) and low energy consumption. Electrical framework heating was successfully exploited for the thermal regeneration of BN, with less than 10% loss in organosulfur capacity over five regeneration cycles.

More generally, our study demonstrates how to produce highly efficient BN sorbents with commercially relevant performance parameters (capacity, selectivity, recyclability), likely to inform other BN sorption applications, such as water treatment or carbon capture. The concept of direct electrical framework heating is highly interesting for rapid and energy-efficient temperature control in other sorbent and catalysts systems (e.g. metal and metal oxide NPs). Moreover, the hybridisation of electrically-insulating materials with electrically-conducting 3D nanocarbon networks can be extended to introduce other new functionalities, such as electrical stimulation, actuation or control of electrical potential. Our synthetic strategy is readily transferable to other 3D nanocarbon frameworks (graphene aerogels, carbon fibre foams) as well as to inorganic materials, produced via high-temperature reactions (e.g. dichalcogenides, carbides, nitrides), opening up routes to a range of new functional porous materials that combine electrical conductivity, thermal stability and mechanical robustness.

### **Conflicts of interest**

There are no conflicts to declare.

### **Acknowledgements**

This research was sponsored by the China Scholarship Council and the University of Leeds. We would like to thank Jennie Dickinson and Mary Bayana for their help with the GC measurements.

### **NOTES AND REFERENCES**

1. Y. Song, D. Mandelli, O. Hod, M. Urbakh, M. Ma and Q. Zheng, *Nature materials*, 2018, 17, 894.
2. X. Xu, Q. Zhang, M. Hao, Y. Hu, Z. Lin, L. Peng, T. Wang, X. Ren, C. Wang and Z. Zhao, *Science*, 2019, 363, 723-727.
3. G. Li, M. Zhu, W. Gong, R. Du, A. Eychmüller, T. Li, W. Lv and X. Zhang, *Advanced Functional Materials*, 2019, 1900188.
4. J. Yin, J. Li, Y. Hang, J. Yu, G. Tai, X. Li, Z. Zhang and W. Guo, *Small*, 2016, 12, 2942-2968.
5. K. N. Yun, Y. Sun, J. S. Han, Y.-H. Song and C. J. Lee, *ACS Applied materials & interfaces*, 2017, 9, 1562-1568.
6. R. Frisenda, E. Navarro-Moratalla, P. Gant, D. P. De Lara, P. Jarillo-Herrero, R. V. Gorbachev and A. Castellanos-Gomez, *Chemical Society Reviews*, 2018, 47, 53-68.
7. Y. Xue, P. Dai, X. Jiang, X. Wang, C. Zhang, D. Tang, Q. Weng, X. Wang, A. Pakdel and C. Tang, *Journal of Materials Chemistry A*, 2016, 4, 1469-1478.
8. P. Wu, W. Zhu, Y. Chao, J. Zhang, P. Zhang, H. Zhu, C. Li, Z. Chen, H. Li and S. Dai, *Chemical Communications*, 2016, 52, 144-147.

9. S. Byun, J. H. Kim, S. H. Song, M. Lee, J. J. Park, G. Lee, S. H. Hong and D. Lee, *Chemistry of Materials*, 2016, 28, 7750-7756.
10. D. R. Deng, F. Xue, C. D. Bai, J. Lei, R. Yuan, M. S. Zheng and Q. F. Dong, *ACS nano*, 2018, 12, 11120-11129.
11. F. An, X. Li, P. Min, H. Li, Z. Dai and Z. Z. Yu, *Carbon*, 2018, 126, 119-127.
12. Y. J. Jeong and M. F. Islam, *Nanoscale*, 2015, 7, 12888-12894.
13. J. Yang, L. S. Tang, R. Y. Bao, L. Bai, Z. Y. Liu, W. Yang, B. H. Xie and M. B. Yang, *Journal of Materials Chemistry A*, 2016, 4, 18841-18851.
14. R. Menzel, D. Iruretagoyena, Y. Wang, S. M. Bawaked, M. Mokhtar, S. A. Al-Tabaiti, S. N. Basahel and M. S. Shaffer, *Fuel*, 2016, 181, 531-536.
15. J. Xiong, W. Zhu, H. Li, L. Yang, Y. Chao, P. Wu, S. Xun, W. Jiang, M. Zhang and H. Li, *Journal of Materials Chemistry A*, 2015, 3, 12738-12747.
16. R. Neubauer, C. Weinlaender, N. Kienzl, B. Bitschnau, H. Schroettner and C. Hochenauer, *Journal of Power Sources*, 2018, 385, 45-54.
17. J. M. Palomino, D. T. Tran, J. L. Hauser, H. Dong and S. R. Oliver, *Journal of Materials Chemistry A*, 2014, 2, 14890-14895.
18. R. Dehghan and M. Anbia, *Fuel Processing Technology*, 2017, 167, 99-116.
19. J. Kou, C. Lu, W. Sun, L. Zhang and Z. Xu, *ACS Sustainable Chemistry & Engineering*, 2015, 3, 3053-3061.
20. B. Liu, Y. Zhu, S. Liu and J. Mao, *Journal of Chemical & Engineering Data*, 2012, 57, 1326-1330.
21. S. Aslam, F. Subhan, Z. Yan, U. Etim and J. Zeng, *Chemical Engineering Journal*, 2017, 315, 469-480.
22. P. Tan, D. M. Xue, J. Zhu, Y. Jiang, Q. X. He, Z. Hou, X. Q. Liu and L. B. Sun, *AIChE Journal*, 2018, 64, 3786-3793.
23. Q. X. He, Y. Jiang, P. Tan, X. Q. Liu, J. X. Qin and L. B. Sun, *ACS Applied Materials & Interfaces*, 2017, 9, 29445-29450.
24. P. Tan, Y. Jiang, L. B. Sun, X. Q. Liu, K. AlBahily, U. Ravon and A. Vinu, *Journal of Materials Chemistry A*, 2018, 6, 23978-24012.
25. J. Xiong, L. Yang, Y. Chao, J. Pang, P. Wu, M. Zhang, W. Zhu and H. Li, *Green Chemistry*, 2016, 18, 3040-3047.
26. J. Xiong, W. Zhu, H. Li, W. Ding, Y. Chao, P. Wu, S. Xun, M. Zhang and H. Li, *Green Chemistry*, 2015, 17, 1647-1656.
27. R. Neubauer, N. Kienzl, B. Bitschnau, H. Schroettner and C. Hochenauer, *Energy & fuels*, 2017, 31, 12942-12950.
28. F. Sharif, L. R. Gagnon, S. Mulmi and E. P. Roberts, *Water Research*, 2017, 114, 237-245.
29. M. Pan, C. Shan, X. Zhang, Y. Zhang, C. Zhu, G. Gao and B. Pan, *Environmental science & technology*, 2017, 52, 739-746.

30. M. Yan, Q. Jiang, T. Zhang, J. Wang, L. Yang, Z. Lu, H. He, Y. Fu, X. Wang and H. Huang, *Journal of Materials Chemistry A*, 2018, 6, 18165-18172.
31. J. Liu, X. Ge, X. Ye, G. Wang, H. Zhang, H. Zhou, Y. Zhang and H. Zhao, *Journal of Materials Chemistry A*, 2016, 4, 1970-1979.
32. K. He, G. Chen, G. Zeng, A. Chen, Z. Huang, J. Shi, T. Huang, M. Peng and L. Hu, *Applied Catalysis B: Environmental*, 2018, 228, 19-28.
33. R. Menzel, S. Barg, M. Miranda, D. B. Anthony, S. M. Bawaked, M. Mokhtar, S. A. Al-Thabaiti, S. N. Basahel, E. Saiz and M. S. Shaffer, *Advanced Functional Materials*, 2015, 25, 28-35.
34. S. Marchesini, C. M. McGilvery, J. Bailey and C. Petit, *ACS Nano*, 2017, 11, 10003-10011.
35. J. Xiong, L. Yang, Y. Chao, J. Pang, M. Zhang, W. Zhu and H. Li, *ACS Sustainable Chemistry & Engineering*, 2016, 4, 4457-4464.
36. X. Zhao, W. Yao, W. Gao, H. Chen and C. Gao, *Advanced Materials*, 2017, 29, 1701482.
37. M. Florent and T. J. Bandosz, *Journal of Materials Chemistry A*, 2018, 6, 3510-3521.
38. C. Yang, J. Wang, Y. Chen, D. Liu, S. Huang and W. Lei, *Nanoscale*, 2018, 10, 10979-10985.
39. I. Esteve-Adell, J. He, F. Ramiro, P. Atienzar, A. Primo and H. García, *Nanoscale*, 2018, 10, 4391-4397.
40. T. Fukumaru, T. Fujigaya and N. Nakashima, *Scientific Reports*, 2015, 5, 7951.
41. T. Kim, J. Hur and S. Jeon, *Semiconductor Science and Technology*, 2016, 31, 055014.
42. S. A. Ganiyu, O. O. Ajumobi, S. A. Lateef, K. O. Sulaiman, I. A. Bakare, M. Qamaruddin and K. Alhooshani, *Chemical Engineering Journal*, 2017, 321, 651-661.
43. P. Tan, J. X. Qin, X. Q. Liu, X. Q. Yin and L. B. Sun, *Journal of Materials Chemistry A*, 2014, 2, 4698-4705.
44. Y. N. Prajapati and N. Verma, *Fuel*, 2017, 189, 186-194.
45. A. Samokhvalov, E. C. Duin, S. Nair and B. J. Tatarchuk, *Applied Surface Science*, 2011, 257, 3226-3232.
46. H. Li, W. Zhu, S. Zhu, J. Xia, Y. Chang, W. Jiang, M. Zhang, Y. Zhou and H. Li, *AIChE Journal*, 2016, 62, 2087-2100.

## FIGURES

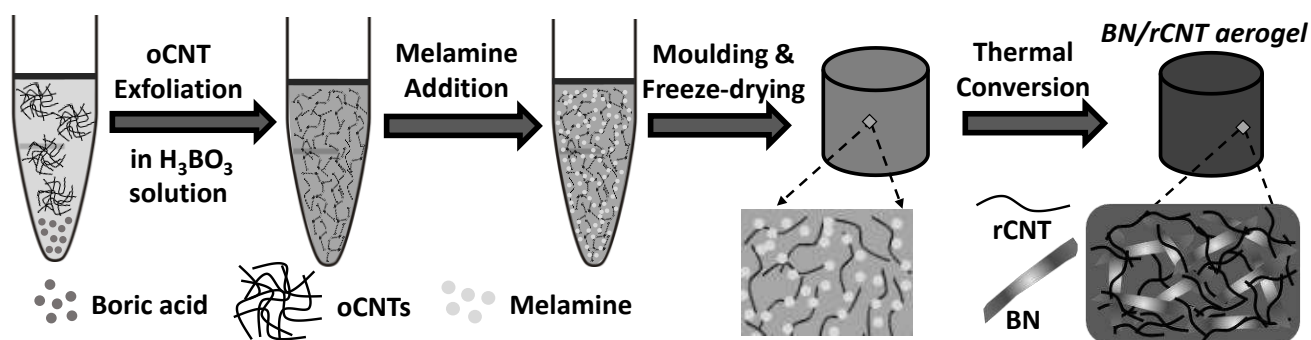


Figure 1. Synthesis of BN/rCNT aerogels via high-temperature conversion of B- and N-containing precursors supported within a CNT aerogel network.

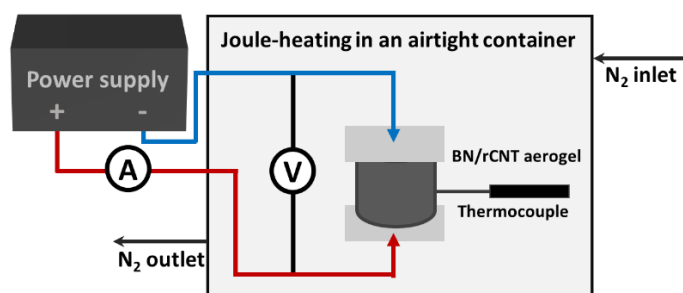


Figure 2. Joule heating of a BN/rCNT aerogel in an airtight container in  $N_2$  atmosphere.

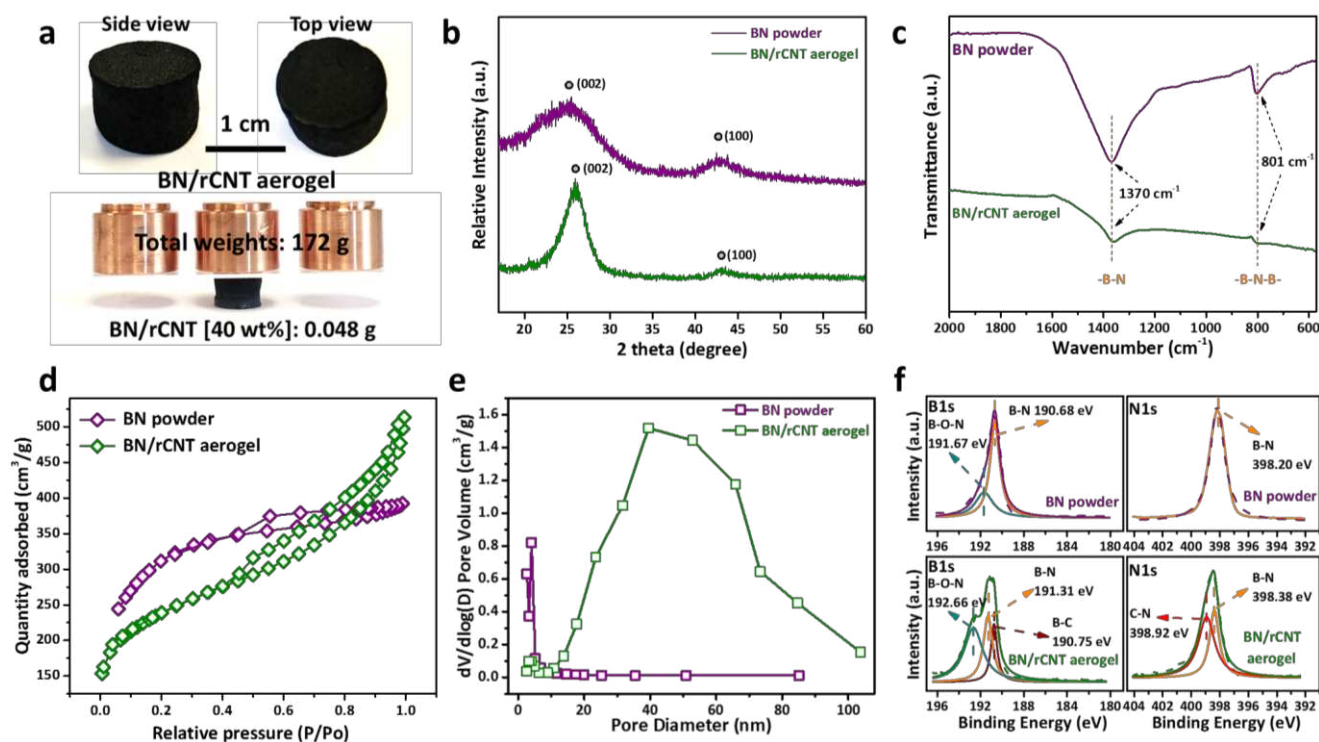
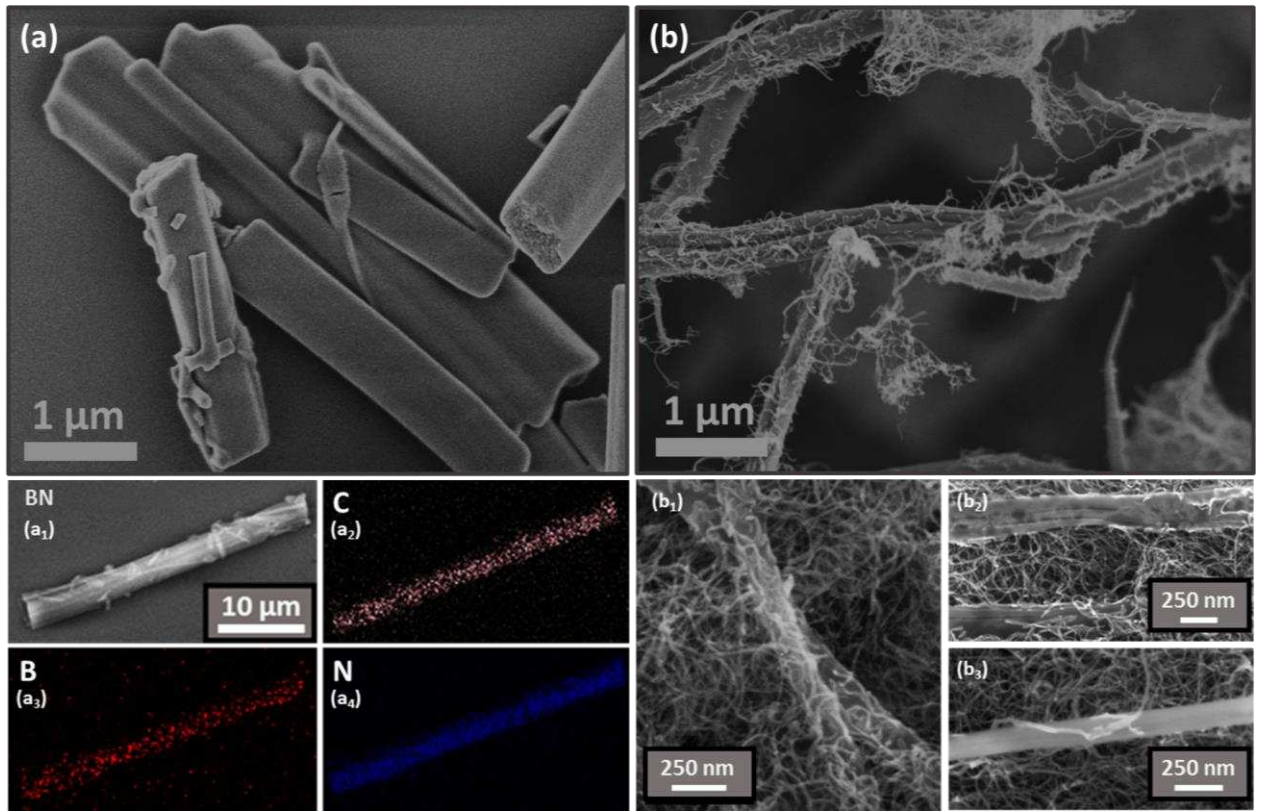
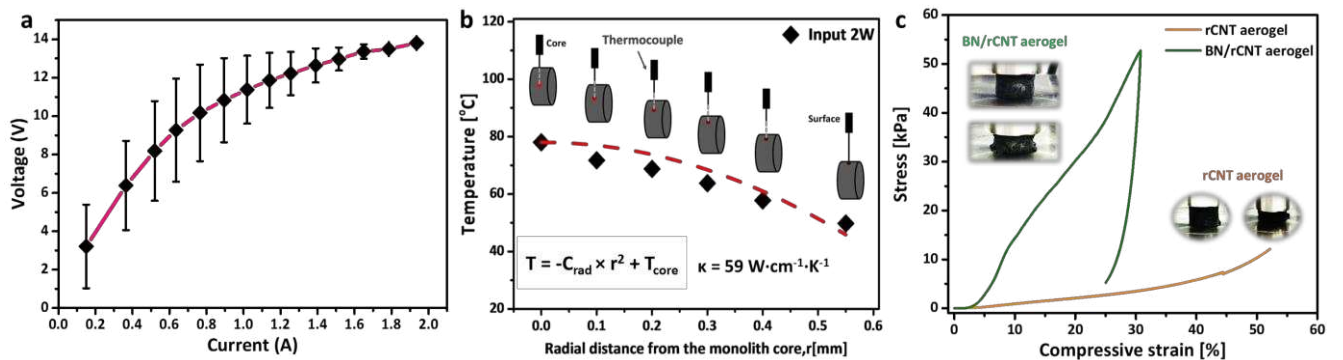


Figure 3. (a) Digital images of BN/rCNT aerogels; (b) Powder XRD patterns of BN powder and BN/rCNT aerogel; (c) IR spectra of BN and BN/rCNT aerogel; (d)  $N_2$  adsorption isotherms and (e) BJH pore distributions of BN powder and BN/rCNT aerogel. (f) XPS analysis (B1s high-resolution scan; N1s high-resolution scan) of BN powder and BN/rCNT aerogel.



**Figure 4.** (a) SEM image of BN powder adsorbent. (a<sub>1</sub> - a<sub>4</sub>) EDX mapping of C, B and N distribution across an individual in-hybridised BN structure. (b) SEM image of BN/rCNT aerogel adsorbent. (b<sub>1</sub> - b<sub>3</sub>) High magnification SEM of BN/rCNT aerogel internal structure.



**Figure 5.** (a) I-V curve of BN/rCNT aerogel. (b) Radial thermal gradient of an uninsulated BN/rCNT aerogel (Joule-heated at 2W), used for the calculation of the thermal conductivity,  $\kappa$ , of the hybrid aerogel. (c) Compressibility measurements of BN/rCNT aerogel and pure rCNT aerogel.

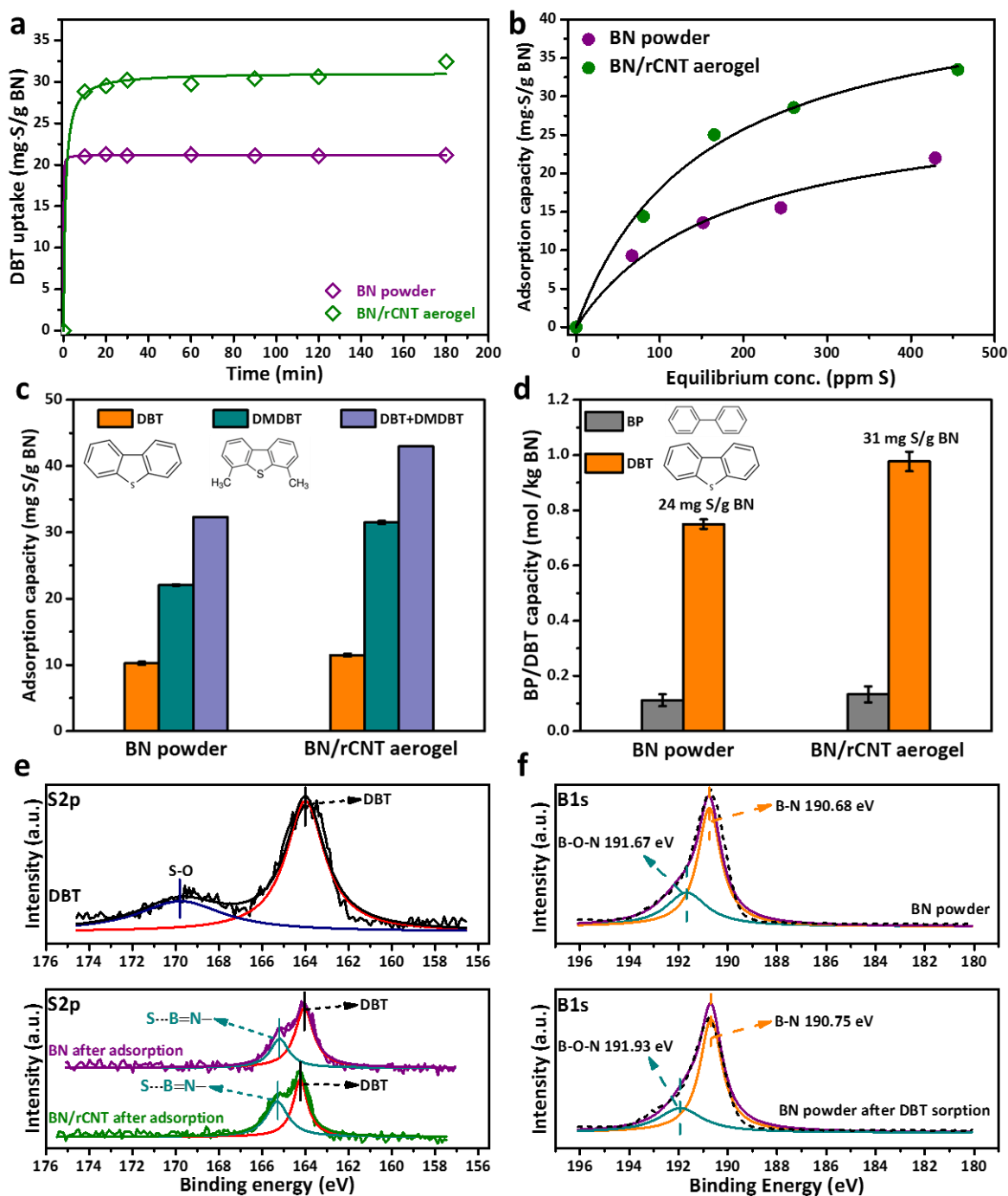


**Figure 6.** (a) DBT adsorption kinetics of BN powder and BN/rCNT aerogel (DBT, 500 ppm S, *n*-octane). (b) DBT adsorption isotherms of BN powder and BN/rCNT aerogel (100 ppm S, 200 ppm S, 300 ppm S and 500 ppm S DBT in *n*-octane). (c) DMTBT adsorption performance of BN powder and BN/rCNT aerogel in the presence of DBT (250 ppm S DMTBT and 250 ppm S DBT in *n*-octane). (d) Selectivity: Adsorption capacities of BN powder and BN/rCNT aerogel as measured in BP/DBT mixtures (2873 ppm BP, 500ppm S DBT in *n*-octane). (e-f) Post-sorption XPS analysis: (e) S2p XPS peaks of DBT powder, BN powder after DBT adsorption and BN/rCNT aerogel after DBT adsorption; (f) B1s XPS peak of BN powder before and after DBT sorption.

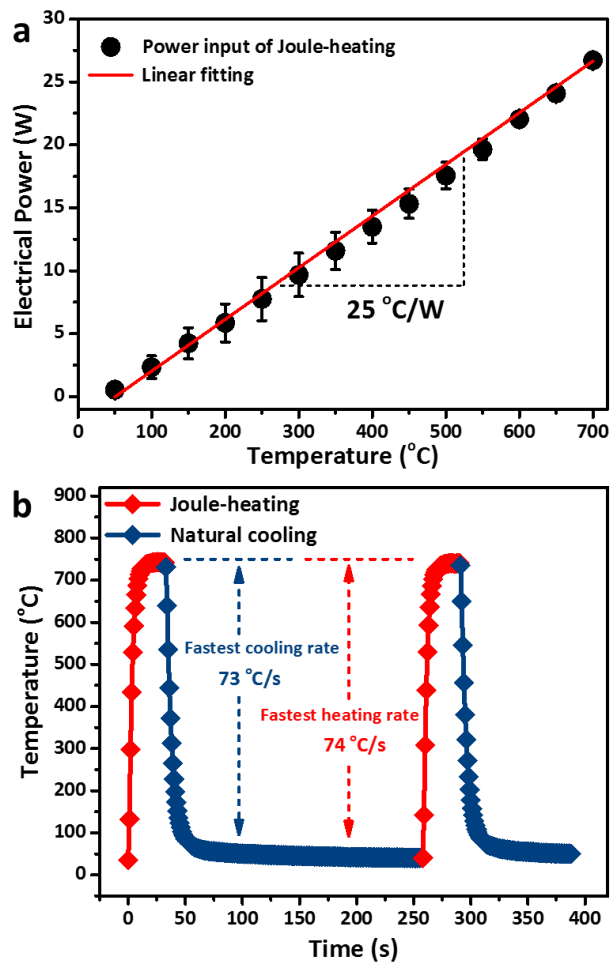


Figure 7. (a) Electrical power versus Joule-heating temperature. (b) Heating and cooling curves of the Joule-heated BN/rCNT aerogel.

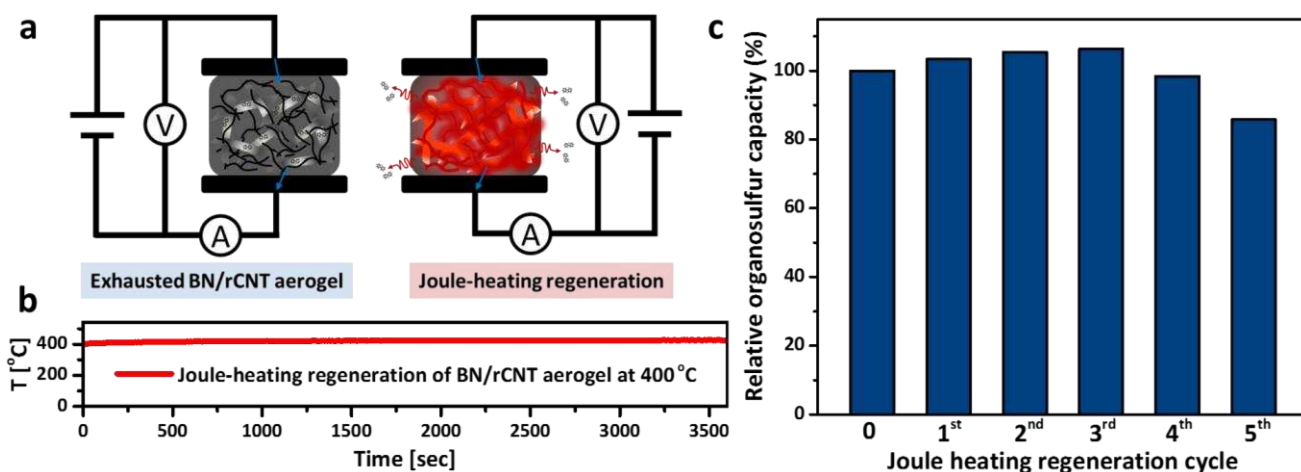


Figure 8. (a) Joule-heating regeneration of an exhausted BN/rCNT aerogel adsorbent via thermal DBT desorption under Joule-heating. (b) Temperature stability over 1 h of Joule-heating regeneration. (c) Regeneration stability of BN/rCNT aerogel adsorbent: Organosulfur uptake (relative to initial organosulfur capacity) over five Joule-heating regeneration cycles.

## TABLES

**Table 1.** Organosulfur Uptake and materials characterisation of BN powder and BN/rCNT aerogel.

Adsorbent	<i>DBT Uptake</i>	<i>Surface Area</i>	<i>Meso-Porosity</i>		<i>Conductivity</i>
	$q_m^a$ (mg·S/g BN)	$S_{BET}^b$ (m <sup>2</sup> /g)	$V_p^c$ (cm <sup>3</sup> /g)	$D_p^d$ (nm)	$\sigma^e$ (S/m)
BN powder	29.6	1004	0.04	4	non-conducting
BN/rCNT aerogel	45.2	840	0.62	40	5.92

<sup>a</sup> Maximum DBT adsorption capacities as extrapolated from Langmuir model (see Fig. 6b); <sup>b</sup> BET specific surface area; <sup>c</sup> BJH meso-pore volume; <sup>d</sup> Average meso-pore size from BJH analysis (see Fig. 3e); <sup>e</sup> Electrical conductivity.

**Table 2.** Organosulfur uptake of various ADS adsorbents.

<b>Adsorbents</b>	<b>S conc. (ppm)</b>	<b>Sorption capacity (mg·S/g ads)</b>	<b>Ref.</b>
<b>MgAl-MMO <sup>a</sup></b>	<b>50 ppm</b>	<b>1.5</b>	<b>14</b>
<b>Cu<sup>+</sup>/MIL-(Fe) <sup>b</sup></b>	<b>50 ppm</b>	<b>11</b>	<b>23</b>
<b>N-doped C</b>	<b>115 ppm</b>	<b>93</b>	<b>22</b>
<b>AC <sup>c</sup></b>	<b>300 ppm</b>	<b>7</b>	<b>42</b>
<b>Cu<sub>2</sub>O</b>	<b>550 ppm</b>	<b>11</b>	<b>19</b>
<b>NaY <sup>d</sup></b>	<b>500 ppm</b>	<b>13</b>	<b>24</b>
<b>ZnY</b>	<b>500 ppm</b>	<b>15</b>	<b>24</b>
<b>Ag/Fe@SiO<sub>2</sub></b>	<b>663 ppm</b>	<b>5</b>	<b>43</b>
<b>Ni-ACB <sup>e</sup></b>	<b>800 ppm</b>	<b>27</b>	<b>44</b>
<b>Cu-BTC <sup>f</sup></b>	<b>630 ppm</b>	<b>32</b>	<b>20</b>
<b>BN/rCNT</b>	<b>500 ppm</b>	<b>32</b>	<b>Here</b>

<sup>a</sup> MMO = mixed metal oxides; <sup>b</sup> Cu<sup>+</sup>/MIL= Cu<sup>+</sup> in MOF; <sup>c</sup> AC = activated carbon;